Photochemical & Photobiological Sciences

PAPER

Cite this: *Photochem. Photobiol. Sci.*, 2018, **17**, 375

Copper(I) and silver(I) complexes of 9,9-dimethyl-4,5-bis(di-*tert*-butylphosphino)xanthene: photophysical properties and structural rigidity under pressure†

Sarah Keller, Alessandro Prescimone, Edwin C. Constable and Catherine E. Housecroft *

Received 23rd November 2017,
Accepted 19th January 2018

DOI: 10.1039/c7pp00432j

rsc.li/pps

The heteroleptic complexes [Cu(*t*Bu-xantphos)(bpy)][PF_6] and [Ag(*t*Bu-xantphos)(bpy)][PF_6], where *t*Bu-xantphos = 9,9-dimethyl-4,5-bis(di-*tert*-butylphosphino)xanthene and bpy = 2,2′-bipyridine have been synthesized and their photophysical properties investigated. Single crystal X-ray diffraction studies of the compounds under ambient and increased pressure are presented; increase in pressure results in little structural perturbation. For the copper(I) complexes, the effects of changing the N^N ligand from bpy to 6-methyl-2,2′-bipyridine (6-Mebpy), 6-bromo-2,2′-bipyridine (6-Brbpy), and 4,4′-di(*tert*-butyl)-2,2′-bipyridine (4,4′-*t*Bu_2bpy) were also investigated. Emissions from the copper(I) complexes are weak, both in solution and the solid state and this is attributed to vibrational quenching effects of the *tert*-butyl substituents of the *t*Bu-xantphos ligands.

Introduction

Luminescent devices include light-emitting diodes (LEDs), organic light-emitting diodes (OLEDs) and light-emitting electrochemical cells (LECs) and are part of the solid state lighting (SSL) technology. The latter is increasingly replacing traditional lighting systems and has revolutionized screen technology for, for example, smartphones, computers and televisions.[1–4] The emissive materials for LECs and OLEDs can be polymers, molecular organics or ionic transition metal complexes (iTMCs).[5] For iTMC devices, copper(I) based compounds have increasingly gained interest due to the high Earth-abundance of copper and its low cost, and the fact that both the singlet and the triplet excited states can be harvested *via* thermally activated delayed fluorescence (TADF).[6,7] Complexes where the copper centre is coordinated by a combination of a P^P chelating ligand (*e.g.* bis(2-(diphenylphosphino)phenyl) ether (POP) or 4,5-bis(diphenylphosphino)-9,9-dimethylxanthene (xantphos)) and an N^N ligand such as 2,2′-bipyridines (bpy) or phenanthrolines with varying substituents, are a particularly interesting class of emitters for LECs[8] and OLEDs.[9] They often exhibit high photoluminescence quantum yields (PLQYs) of up to 70% in the solid state and, when used as emitters in LECs, luminance values of 145 cd m^{-2} and device lifetimes of ~80 h have been achieved.[10,11] For the design of the emissive copper(I) complexes, the stabilization of the tetrahedral geometry plays a crucial role in avoiding quenching processes and increasing the PLQYs and excited state lifetimes.[12] Substituents in the 6-positions of the bpy, for example alkyl or CF_3 groups, prevent the tetrahedron from flattening, make the structure more rigid and improve the emissive properties of the complex.[11,13,14]

We have been interested in the effect of a change in the steric and electronic properties of the chelating bisphosphane and decided to investigate the potential of 9,9-dimethyl-4,5-bis(di-*tert*-butylphosphino)xanthene (*t*Bu-xantphos) as the chelating bisphosphane. The disadvantage of alkyl phosphanes, as opposed to aryl phosphanes, is that they are prone to oxidation to phosphane oxides. However, we hoped that the sterically hindered *t*Bu_2P groups would not only shield the copper centre and stabilize the tetrahedral geometry, but would in addition decrease the tendency for phosphane oxidation.

The ligand *t*Bu-xantphos is often used for catalysis in combination with different metals, for example in the copper-catalysed alkylboration of alkenes.[15] However, there are very few cases in which metal complexes containing *t*Bu-xantphos have been isolated and characterized. Examples are the rhodium complex [(*t*Bu-xantphos)RhCl] and its hydride, [(*t*Bu-xantphos)RhH_2Cl].[16] For group 11, no complexes with copper or silver and *t*Bu-xantphos have been described although the complex

Department of Chemistry, University of Basel, BPR 1096, Mattenstrasse 24a, CH-4058 Basel, Switzerland. E-mail: catherine.housecroft@unibas.ch

† Electronic supplementary information (ESI) available. CCDC 1583820–1583822, 1583828, 1583832–1583835, 1583842–1583845. For ESI and crystallographic data in CIF or other electronic format see DOI: 10.1039/c7pp00432j

[{*t*Bu-xantphos}AuCl] has been successfully used as a catalyst to transform C–F to C–X bonds (X = O, S, N).[17]

It has previously been established that silver complexes with the motif $[Ag(P^P)(N^N)]^+$ show reasonable emissive properties and promising results in LECs[18] and recently a silver complex with excellent TADF properties and PLQY of 100% was reported,[19] which motivated us to investigate the analogous Ag^+ complex with *t*Bu-xantphos and bpy.

Experimental

General

^{1}H, ^{13}C and ^{31}P NMR spectra were recorded at room temperature using a Bruker Avance III-500 or III-400 NMR spectrometer. ^{1}H and ^{13}C NMR chemical shifts were referenced to residual solvent peaks with respect to δ(TMS) = 0 ppm and ^{31}P NMR chemical shifts with respect to δ(85% aqueous H_3PO_4) = 0 ppm. Solution absorption and emission spectra were measured using an Agilent 8453 spectrophotometer and a Shimadzu RF-5301PC spectrofluorometer, respectively. Electrospray ionization (ESI) mass spectra were recorded on a Shimadzu LCMS-2020 instrument. Quantum yields were measured using a Hamamatsu absolute photoluminescence (PL) quantum yield spectrometer C11347 Quantaurus-QY. Emission lifetimes and powder emission spectra were measured with a Hamamatsu Compact Fluorescence lifetime Spectrometer C11367 Quantaurus-Tau, using an LED light source with λ_{exc} = 365 nm.

$[Cu(MeCN)_4][PF_6]$[20] and 6-Mebpy[21] were prepared following literature methods, *t*Bu-xantphos was purchased from Strem chemicals, bpy from Apollo Scientific, 6-Brbpy from TCI, 4,4′-tBu$_2$bpy from Sigma-Aldrich and $Ag[PF_6]$ from Fluorochem. All chemicals were used as received.

[Cu(*t*Bu-xantphos)(bpy)][PF$_6$]. Under nitrogen, a solution of *t*Bu-xantphos (75 mg, 0.15 mmol, 1.0 eq.) in dry CH_2Cl_2 (10 ml) was added to a solution of $[Cu(MeCN)_4][PF_6]$ (56 mg, 0.15 mmol, 1.0 eq.) in dry CH_2Cl_2 (5 ml). The colourless solution was stirred for 2 h. A solution of bpy (23 mg, 0.15 mmol, 1.0 eq.) in dry CH_2Cl_2 (5 ml) was added to the mixture and the resulting yellow solution was stirred for two hours. All volatiles were removed *in vacuo* and the residue was washed with hexane to yield [Cu(*t*Bu-xantphos)(bpy)]PF_6 (69 mg, 0.08 mmol, 53%) as yellow powder. ^{1}H NMR (500 MHz, CD_2Cl_2, 298 K) δ/ppm 8.72 (d, J = 4.3 Hz, 2H, H^{A6}), 8.40 (dt, J = 8.0, 0.9 Hz, 2H, H^{A3}), 7.89 (td, J = 7.8, 1.8 Hz, 2H, H^{A4}), 7.73 (dd, J = 7.8, 1.4 Hz, 2H, H^{C5}), 7.71–7.65 (m, 2H, H^{C3}), 7.369 (t, J = 7.7 Hz, 2H, H^{A5}), 7.366 (dd, J = 7.5, 1.1 Hz, 2H, H^{C4}), 1.67 (s, 6H, $H^{xantphos\text{-}Me}$), 1.34–1.29 (m, 36H, H^{tBu}). ^{13}C NMR (126 MHz, CD_2Cl_2, 298 K) δ/ppm 155.5 (C^{A2}), 154.3 (t, J = 5.6 Hz, C^{C1}), 149.9 (C^{A6}), 137.9 (C^{A4}), 133.6 (t, J = 1.8 Hz, C^{C6}), 133.3 (C^{C3}), 129.7 (C^{C5}), 125.2 (C^{C4}), 124.9 (C^{A5}), 121.9(C^{A3}), 118.3 (t, J = 11.5 Hz, C^{C2}), 36.2 ($C^{xantphos\text{-}bridge}$), 35.6 (t, J = 7.3 Hz, $C^{tBu\text{-}quat}$), 31.0 (t, J = 4.4 Hz, C^{tBu}), 30.3 ($C^{xantphos-Me}$). $^{31}P\{^1H\}$ NMR (202 MHz, CD_2Cl_2, 298 K) δ/ppm 20.6 (broad, FWHM = 110 Hz), −144.5 (sept, J_{PF} = 710 Hz, $[PF_6]^-$). ESI MS: m/z 561.1 $[Cu(tBu\text{-xantphos})]^+$ (base peak, calc. 561.3, base peak for $[Cu(tBu\text{-xantphos})(bpy)]^+$, calc. 717.3). Found C 56.73, H 6.68, N 3.41; $C_{41}H_{56}CuF_6N_2OP_3$ requires C 57.04, H 6.54, N 3.24%.

[Cu(*t*Bu-xantphos)(6-Mebpy)][PF$_6$]. (SK167). Under nitrogen, a solution of *t*Bu-xantphos (75 mg, 0.15 mmol, 1.0 eq.) in dry CH_2Cl_2 (10 ml) was added to a solution of $[Cu(MeCN)_4][PF_6]$ (56 mg, 0.15 mmol, 1.0 eq.) in dry CH_2Cl_2 (5 ml). The colourless solution was stirred for 2 h. A solution of 6-Mebpy (26 mg, 0.15 mmol, 1.0 eq.) in dry CH_2Cl_2 (5 ml) was added to the mixture and the resulting yellow solution was stirred for two hours. All volatiles were removed *in vacuo* and the residue was washed with hexane to yield [Cu(xant-*t*Bu-phos)(6-Mebpy)]PF_6 (78 mg, 0.09 mmol, 60%) as yellow solid. ^{1}H NMR (500 MHz, CD_2Cl_2, 298 K) δ/ppm 8.64 (d, J = 4.1 Hz, 1H, H^{A6}), 8.43 (dt, J = 8.0, 0.9 Hz, 1H, H^{A3}), 8.21 (d, J = 7.8 Hz, 1H, H^{B3}), 7.81 (td, J = 7.8, 1.8 Hz, 1H, H^{A4}), 7.75 (dd, J = 7.8, 1.4 Hz, 2H, H^{C5}), 7.73–7.69 (m, 1H, H^{B4}), 7.69–7.66 (m, 2H, H^{C3}), 7.39 (t, J = 7.8 Hz, 2H, H^{C4}), 7.30 (ddd, J = 7.4, 4.8, 1.0 Hz, 1H, H^{A5}), 7.19 (d, J = 7.6 Hz, 1H, H^{B5}), 2.61 (s, 3H, H^{Me}), 1.66 (s, 6H, $H^{xantphos\text{-}Me}$), 1.42–1.39 (m, 36H, H^{tBu}). ^{13}C NMR (126 MHz, CD_2Cl_2, 298 K) δ/ppm 158.5 (C^{B6}), 156.8 (C^{A2}), 155.8 (C^{B2}), 154.0 (t, J = 5.6 Hz, C^{C1}), 149.6 (C^{A6}), 137.5 (C^{B4}), 137.3 (C^{A4}), 133.5 (t, J = 2.0 Hz, C^{C6}), 133.3 (C^{C3}), 130.1 (C^{C5}), 125.3 (t, J = 2.5 Hz, C^{C4}), 124.1 (C^{A5}), 123.8 (C^{B5}), 121.4 (C^{A3}), 118.4 (C^{B3}), 117.6 (t, J = 13.5 Hz, C^{C2}), 36.2 (t, J = 1.1 Hz, $C^{xantphos\text{-}bridge}$), 35.5 (t, J = 8.4 Hz, $C^{tBu\text{-}quat}$), 30.9 (t, J = 4.3 Hz, C^{tBu}), 30.5 ($C^{xantphos\text{-}Me}$), 25.0 (C^{Me}). $^{31}P\{^1H\}$ NMR (202 MHz, CD_2Cl_2, 298 K) δ/ppm 22.1 (broad, FWHM = 63 Hz), −144.5 (sept, J_{PF} = 710 Hz, $[PF_6]^-$). ESI MS: m/z 561.4 $[Cu(tBu\text{-xantphos})]^+$ (base peak, calc. 561.3, base peak for $[Cu(tBu\text{-xantphos})(6\text{-Mebpy})]^+$, calc. 731.3). Found C 59.72, H 7.28, N 2.90; $C_{42}H_{58}CuF_6N_2OP_3{\cdot}C_6H_{14}$ requires C 59.83, H 7.53, N 2.91%.

[Cu(*t*Bu-xantphos)][PF$_6$]. In an attempt to prepare [Cu(*t*Bu-xantphos)(6-Brbpy)][PF_6], [Cu(*t*Bu-xantphos)][PF_6] was isolated. Under nitrogen, a solution of *t*Bu-xantphos (75 mg, 0.15 mmol, 1.0 eq.) in dry CH_2Cl_2 (10 ml) was added to a solution of $[Cu(MeCN)_4][PF_6]$ (56 mg, 0.15 mmol, 1.0 eq.) in dry CH_2Cl_2 (5 ml). The colourless solution was stirred for 2 h. A solution of 6-Brbpy (35 mg, 0.15 mmol, 1.0 eq.) in dry CH_2Cl_2 (5 ml) was added to the mixture and the resulting yellow solution was stirred for two hours. All volatiles were removed *in vacuo* and the residue was washed with hexane to yield a pale orange solid (82 mg) which was identified as a mixture of [Cu(*t*Bu-xantphos)][PF_6] and 6-Brbpy. The ^{1}H and ^{13}C NMR resonances assigned to free 6-Brbpy matched those reported.[22] [Cu(*t*Bu-xantphos)][PF_6]: ^{1}H NMR (500 MHz, CD_2Cl_2, 298 K) δ/ppm 7.74 (dd, J = 7.8, 1.3 Hz, 2H, H^{C5}), 7.69–7.66 (m, 2H, H^{C3}), 7.38 (t, J = 7.8 Hz, 2H, H^{C4}), 1.65 (s, 6H, $H^{xantphos\text{-}Me}$), 1.42–1.39 (m, 36H, H^{tBu}). ^{13}C NMR (126 MHz, CD_2Cl_2, 298 K) δ/ppm 154.1 (t, J_{PC} = 5.6 Hz, C^{C1}), 133.7 (t, J_{PC} = 2.0 Hz, C^{C6}), 133.3 (C^{C3}), 130.0 (C^{C5}), 125.3 (t, J_{PC} = 2.5 Hz, C^{C4}), 117.5 (t, J_{PC} = 13.6 Hz, C^{C2}), 36.2 ($C^{xantphos\text{-}Me}$), 35.4 (t, J = 8.4 Hz, $C^{tBu\text{-}quat}$), 30.8 (t, J = 4.3 Hz, C^{tBu}), 30.2 ($C^{xantphos\text{-}Me}$). $^{31}P\{^1H\}$ NMR (202 MHz, CD_2Cl_2, 298 K) δ/ppm 21.7 (broad, FWHM = 57 Hz), −144.5 (sept, J_{PF} =

710 Hz, $[PF_6]^-$). ESI MS: *m*/*z* 561.3 $[Cu(t\text{Bu-xantphos})]^+$ (base peak, calc. 561.3). Insufficient pure material for elemental analysis.

[Cu(*t*Bu-xantphos)(4,4′-*t*Bu$_2$bpy)][PF$_6$]. Under nitrogen, a solution of *t*Bu-xantphos (75 mg, 0.15 mmol, 1.0 eq.) in dry CH_2Cl_2 (10 ml) was added to a solution of $[Cu(MeCN)_4][PF_6]$ (56 mg, 0.15 mmol, 1.0 eq.) in dry CH_2Cl_2 (5 ml). The colourless solution was stirred for 2 h. A solution of 4,4′-*t*Bu$_2$bpy (40 mg, 0.15 mmol, 1.0 eq.) in dry CH_2Cl_2 (5 ml) was added to the mixture and the resulting yellow solution was stirred for two hours. All volatiles were removed *in vacuo* and the residue was washed with hexane to yield $[Cu(t\text{Bu-xantphos})(4,4'\text{-}t\text{Bu}_2\text{bpy})]PF_6$ (116 mg, 0.12 mmol, 80%) as yellow solid. ^{1}H NMR (500 MHz, CD_2Cl_2, 298 K) δ/ppm 8.66 (broad signal, FWHM = 16.6 Hz, 2H, H^{A6}), 8.34 (broad signal, FWHM = 9.2 Hz, 2H, H^{A3}), 7.71 (dd, J = 7.7, 1.3 Hz, 2H, H^{C5}), 7.70–7.67 (m, 2H, H^{C3}), 7.42–7.39 (m, 2H, H^{A5}), 7.34 (t, J = 7.7 Hz, 2H, H^{C4}), 1.68 (s, 6H, $H^{\text{xantphos-Me}}$), 1.40 (s, 18H, $H^{\text{bpy}t\text{Bu}}$), 1.26–1.23 (m, consisting of two singlets and a broad signal in the middle, 36H, $H^{Pt\text{Bu}}$). ^{13}C NMR (126 MHz, CD_2Cl_2, 298 K) δ/ppm 162.6 (C^{A4}), 155.0 (m, C^{A2+C1}), 149.9 (C^{A6}), 133.9 (C^{C6}), 133.3 (C^{C3}), 129.0 (C^{C5}), 124.8 (C^{C4}), 122.4 (m, C^{A5}), 119.0 (m, C^{A3+C2}), 36.3 ($C^{\text{xantphos-bridge}}$), 35.6 (t, J = 6.0 Hz, $C^{t\text{Bu-quat}}$), 31.0 (t, J = 4.5 Hz, $C^{t\text{Bu}}$), 30.8 ($C^{\text{bpy}t\text{Bu}}$), 29.7 ($C^{\text{xantphos-Me}}$). ^{31}P{^{1}H} NMR (202 MHz, CD_2Cl_2, 298 K) δ/ppm 17.7 (broad, FWHM = 180 Hz), −144.5 (sept, J_{PF} = 710 Hz, $[PF_6]^-$). ESI MS: *m*/*z* 561.4 $[Cu(t\text{Bu-xantphos})]^+$ (base peak, calc. 561.3, base peak for $[Cu(t\text{Bu-xantphos})(4,4'\text{-}t\text{Bu}_2\text{bpy})]^+$, calc. 829). Found C 59.65, H 7.74, N 3.06; $C_{49}H_{72}CuF_6N_2OP_3{\cdot}H_2O$ requires C 59.23, H 7.51, N 2.82%.

[Ag(*t*Bu-xantphos)(bpy)][PF$_6$]. Under nitrogen, a solution of *t*Bu-xantphos (75 mg, 0.15 mmol, 1.0 eq.) in dry CH_2Cl_2 (10 ml) was added to a solution of $AgPF_6$ (38 mg, 0.15 mmol, 1.0 eq.) in dry CH_2Cl_2 (5 ml). The colourless solution was stirred for 2 h. A solution of bpy (23 mg, 0.15 mmol, 1.0 eq.) in dry CH_2Cl_2 (5 ml) was added to the mixture and the resulting yellow solution was stirred for two hours. All volatiles were removed *in vacuo* to yield $[Ag(t\text{Bu-xantphos})(bpy)][PF_6]$ (99 mg, 0.11 mmol, 73%) as colourless powder. Small impurities of free *t*Bu-xantphos.

^{1}H NMR (500 MHz, CD_2Cl_2, 298 K) δ/ppm 8.70 (ddd, J = 4.8, 1.8, 0.9 Hz, 2H, H^{A6}), 8.35 (dt, J = 8.0, 1.0 Hz, 2H, H^{A3}), 7.90 (ddd, J = 8.0, 7.6, 1.8 Hz, 2H, H^{A4}), 7.70–7.68 (m, 4H, H^{C3+C5}), 7.39 (ddd, J = 7.5, 4.8, 1.2 Hz, 2H, H^{A5}), 7.31 (t, J = 7.7 Hz, 2H, H^{C4}), 1.63 (s, 6H, $H^{\text{xantphos-Me}}$), 1.33–1.29 (m, consisting of two singlets and a broad signal in the middle, 36H, $H^{t\text{Bu}}$). ^{13}C NMR (126 MHz, CD_2Cl_2, 298 K) δ/ppm 155.7 (C^{A2}), 155.1 (t, J = 5.8 Hz, C^{C1}), 150.2 (C^{A6}), 138.1 (C^{A4}), 133.8 (m, C^{C5+C6}), 129.1 (C^{C3}), 124.8 (C^{A5}), 124.2 (m, C^{C4}), 122.2 (C^{A3}), 118.4 (td, J = 7.9, 3.1 Hz, C^{C2}), 36.0 (m, $C^{\text{xantphos-bridge}}$), 35.6 (m, $C^{t\text{Bu-quat}}$), 31.0 (td, J = 5.3, 0.9 Hz, $C^{t\text{Bu}}$), 30.0 ($C^{\text{xantphos-Me}}$). ^{31}P{^{1}H} NMR (202 MHz, CD_2Cl_2, 298 K) δ/ppm 28.0 (d, $J_{31P-109Ag}$ = 519 Hz), 28.0 (d, $J_{31P-107Ag}$ = 444 Hz), 10.5 (*t*Bu-xantphos, 7%), −144.5 (sept, J_{PF} = 710 Hz, $[PF_6]^-$). ESI MS: *m*/*z* 605.4 $[Ag(t\text{Bu-xantphos})]^+$ (base peak, calc. 605.2, base peak for $[Ag(t\text{Bu-xantphos})(bpy)]^+$, calc. 761.3). Found: C 54.43, H 6.36, N 3.21; $C_{41}H_{56}AgF_6N_2OP_3$ requires C 54.25, H 6.22, N 3.09%.

Crystallography

Ambient pressure data were collected on a Bruker Kappa Apex2 diffractometer with data reduction, solution and refinement using the programs APEX[23] and CRYSTALS.[24] Structural analysis was carried out using Mercury v. 3.9.[25,26] High-pressure single crystal experiments were carried out using a Merrill-Bassett diamond anvil cell[27] (half-opening angle 40°), equipped with Boehler-Almax diamonds with 600 μm culets and a tungsten gasket.[28] Hexane was used as hydrostatic medium and a small ruby chip was loaded into the cell as the pressure calibrant with the ruby fluorescence used to measure the pressure.[29] Diffraction data were collected using synchrotron radiation of wavelength λ = 0.4859 Å at room temperature on a Newport IS4CCD (4 circle) diffractometer with a Pilatus 300 K detector at Station I19 at the Diamond Light Source, Harwell Science and Innovation Campus. Integrations were carried out using the program CrysAlisPro[30] and absorption corrections with the program ABSPACK.[29] Refinements were carried out with CRYSTALS[23] using the ambient pressure structure as starting models.

[Cu(*t*Bu-xantphos)(bpy)][PF$_6$]. $C_{41}H_{56}CuF_6N_2OP_3$, M = 863.36, yellow block, monoclinic, space group $P2_1/c$, a = 12.2247(10), b = 15.0283(12), c = 22.5879(19) Å, β = 98.452(3)°, U = 4104.7(6) Å^3, Z = 4, D_c = 1.397 Mg m^{-3}, μ(Cu-Kα) = 2.385 mm^{-1}, T = 123 K. Total 88 540 reflections, 7254 unique, R_{int} = 0.033. Refinement of 7132 reflections (655 parameters) with $I > 2\sigma(I)$ converged at final R_1 = 0.0331 (R_1 all data = 0.0334), wR_2 = 0.0337 (wR_2 all data = 0.0345), gof = 1.0796. CCDC 1583820.†

For high pressure data and respective CCDC codes see Table S1.†

[Cu(*t*Bu-xantphos)][PF$_6$]·H$_2$O. $C_{31}H_{52}CuF_6O_3P_3$, M = 743.21, yellow plate, orthorhombic, space group $I2mm$, a = 10.6543(8), b = 11.1834(14), c = 15.7615(11) Å, U = 1878.0(3) Å^3, Z = 2, D_c = 1.314 Mg m^{-3}, μ(Cu-Kα) = 2.538 mm^{-1}, T = 123 K. Total 3944 reflections, 1711 unique, R_{int} = 0.034. Refinement of 1698 reflections (126 parameters) with $I > 2\sigma(I)$ converged at final R_1 = 0.1497 (R_1 all data = 0.1505), wR_2 = 0.1635 (wR_2 all data = 0.1639), gof = 1.1082. CCDC 1583821.†

[Ag(*t*Bu-xantphos)(bpy)][PF$_6$]. $C_{41}H_{56}AgF_6N_2OP_3$, M = 907.68, colourless block, triclinic, space group $P\bar{1}$, a = 12.3873(9), b = 12.5363(9), c = 15.3282(12) Å, α = 104.142(3), β = 109.108(2), γ = 103.339(2)°; U = 2051.8(3) Å^3, Z = 2, D_c = 1.469 Mg m^{-3}, μ(Cu-Kα) = 5.576 mm^{-1}, T = 123 K. Total 26 703 reflections, 7397 unique, R_{int} = 0.027. Refinement of 7256 reflections (523 parameters) with $I > 2\sigma(I)$ converged at final R_1 = 0.0383 (R_1 all data = 0.0387), wR_2 = 0.0779 (wR_2 all data = 0.0779), gof = 0.8973. CCDC 1583822.†

For high pressure data and respective CCDC codes see Table S2.†

Results and discussion

Synthesis and characterization of [Cu(*t*Bu-xantphos)(bpy)][PF_6] complexes and [Ag(*t*Bu-xantphos)(bpy)][PF_6]

The syntheses of the [Cu(*t*Bu-xantphos)(N^N)][PF_6] complexes with N^N = bpy, 6-Mebpy and 4,4′-(*t*Bu)$_2$bpy, as well as [Ag(*t*Bu-xantphos)(bpy)][PF_6] were carried out following the standard procedures for [Cu(POP)(N^N)][PF_6] complexes.[14,15,31] An analogous reaction was carried out between [Cu(MeCN)$_4$][PF_6], *t*Bu-xantphos and 6-Brbpy, but, as described below, this reaction failed to produce the desired heteroleptic complex. Since alkyl phosphanes are prone to oxidation (although dialkylbiarylphosphanes were found to be air stable[32]), inert conditions (N_2 atmosphere, dry and degassed solvents) were applied during the reaction as a precaution. The solid products were air stable and were isolated in yields of 53 to 80%. The base peaks in the electrospray mass spectra were assigned to [Cu(*t*Bu-xantphos)]$^+$ for all the copper complexes, or to [Ag(*t*Bu-xantphos)]$^+$. Mass peaks arising from the heteroleptic [Cu(*t*Bu-xantphos)(N^N)]$^+$ cations or [Ag(*t*Bu-xantphos)(bpy)]$^+$ were not detected. Elemental analysis was performed to confirm the purity of the bulk compounds [Cu(*t*Bu-xantphos)(bpy)][PF_6], [Cu(*t*Bu-xantphos)(6-Mebpy)][PF_6], [Cu(*t*Bu-xantphos)(4,4′-*t*Bu$_2$bpy)][PF_6] and [Ag(*t*Bu-xantphos)(bpy)][PF_6]. Unambiguous confirmation of the formation of the heteroleptic complexes came from NMR spectroscopic measurements.

The compounds were analysed by 1- and 2-dimensional NMR spectroscopic techniques (^{1}H, ^{31}P, ^{13}C, COSY, NOESY, HMQC, HMBC), which allowed the unambiguous assignment of all signals. The ^{31}P NMR spectra showed broad signals for the copper complexes and a set of two doublets for [Ag(*t*Bu-xantphos)(bpy)][PF_6] (Fig. 1) in addition to the septet at δ −144.5 ppm arising from [PF_6]$^-$ (not shown).

The NOESY spectra provide an invaluable tool for the confirmation that heteroleptic [Cu(*t*Bu-xantphos)(bpy)][PF_6] species (as opposed to a mixture of homoleptic species or free ligands) are present in solution. Cross peaks between the signal of the *t*Bu groups of *t*Bu-xantphos and proton H^{A6} of bpy (see Scheme 1 for atom labelling) as well as between *t*Bu and the Me group of 6-Mebpy demonstrate a through-space interaction between the two ligands coordinated to the same metal atom. This confirms the formation of [Cu(*t*Bu-xantphos)(bpy)][PF_6], [Ag(*t*Bu-xantphos)(bpy)][PF_6], [Cu(*t*Bu-xantphos)(4,4′-*t*Bu$_2$bpy)][PF_6] and [Cu(*t*Bu-xantphos)(6-Mebpy)][PF_6] (Fig. 2 and Fig. S1 to S9†). For the product of the attempted preparation of [Cu(*t*Bu-xantphos)(6-Brbpy)][PF_6], no cross peaks between H^{A6} and *t*Bu were observed (Fig. S10 and S11†). In this case, the steric hindrance of the *tert*-butyl groups coupled with the size of the bromo substituent prevented coordination of the 6-Brbpy to copper(I). This is further supported by the fact that the signals in the ^{1}H NMR spectrum which were assigned to 6-Brbpy in the complex solution coincide exactly with the signals of a sample of free 6-Brbpy (see Fig. S12†). Furthermore, crystallization of the product

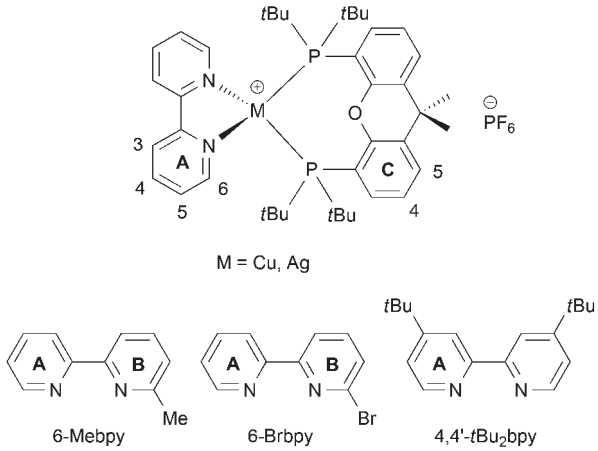

Scheme 1 Structure of the N^N ligands and complexes with ring labels for NMR spectroscopic assignments.

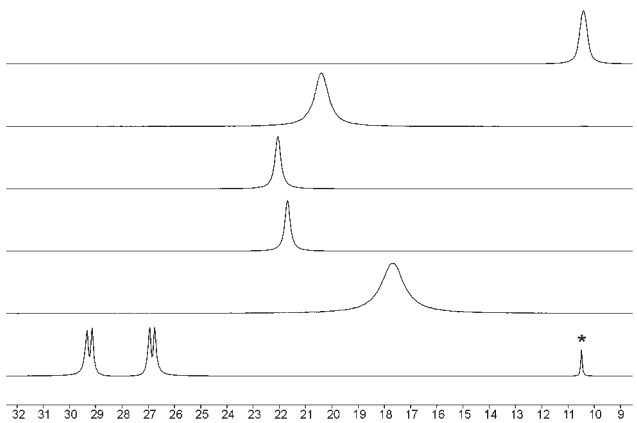

Fig. 1 Parts of the ^{31}P{^{1}H} NMR spectra (202 MHz, 298 K) of CD_2Cl_2 solutions of *t*Bu-xantphos (top), [Cu(*t*Bu-xantphos)(bpy)][PF_6], [Cu(*t*Bu-xantphos)(6-Mebpy)][PF_6], [Cu(*t*Bu-xantphos)][PF_6] with 6-Brbpy, [Cu(*t*Bu-xantphos)(4,4′-*t*Bu$_2$bpy)][PF_6] and [Ag(*t*Bu-xantphos)(bpy)][PF_6] (bottom, signal labelled with an asterisk indicates free *t*Bu-xantphos ligand).

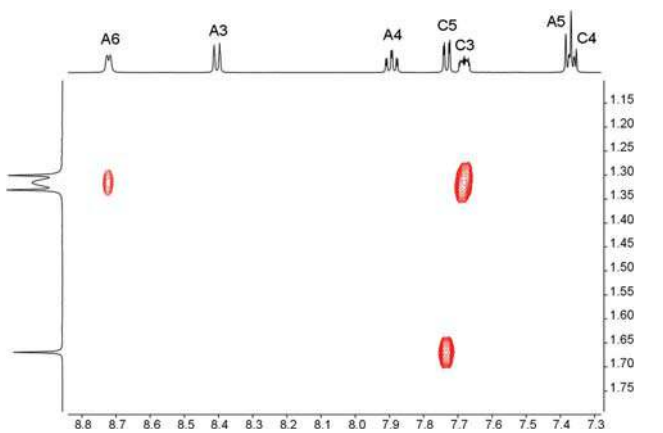

Fig. 2 Part of the NOESY spectrum of [Cu(*t*Bu-xantphos)(bpy)][PF_6] in CD_2Cl_2 at 298 K, 500 MHz. The NOESY cross peak between the *t*Bu signal at δ 1.31 ppm and the H^{A6} signal at δ 8.72 ppm is clearly visible.

obtained from this synthesis yielded single crystals of [Cu(*t*Bu-xantphos)][PF_6] (see crystallography section).

Electrochemistry

For both the electrochemical and photophysical investigations, [Cu(xantphos)(bpy)][PF_6][14] was used as a reference compound. The electrochemical behaviour of the heteroleptic complexes was investigated using cyclic voltammetry (CV), with the voltammogram for [Cu(*t*Bu-xantphos)(bpy)][PF_6] illustrated in Fig. 3 as an example. The oxidation potentials $E^{ox}_{1/2}$ (see Table 1) for [Cu(*t*Bu-xantphos)(bpy)][PF_6] (+0.70 V) and [Cu(*t*Bu-xantphos)(4,4′-*t*Bu$_2$bpy)][PF_6] (+0.62 V) are at lower potentials than for the reference compound [Cu(xantphos)(bpy)][PF_6] (+0.76 V).[14] This indicates that Cu^+/Cu^{2+} oxidation is easier for the complexes with *t*Bu-xantphos than xantphos, and is consistent with the stronger electron-donating character of the *tert*-butyl groups in *t*Bu-xantphos *versus* phenyl groups in xantphos. The differences of 270 mV for [Cu(*t*Bu-xantphos)(bpy)][PF_6] and 370 mV for [Cu(*t*Bu-xantphos)(4,4′-*t*Bu$_2$bpy)][PF_6] between the anodic and cathodic peaks demonstrate the irreversibility or pseudo-reversibility of the oxidation processes. A second oxidation peak (illustrated for [Cu(*t*Bu-xantphos)(bpy)][PF_6] in Fig. 3), was found for all the complexes and is attributed to oxidation of the phosphane ligand. Reduction processes for the compounds were poorly resolved.

For [Ag(*t*Bu-xantphos)(bpy)]$^+$, the oxidation potential of +0.87 V is of a similar order of magnitude as is reported for neutral silver complexes with POP and CF_3-functionalized 2-pyridyl pyrrolides (+0.74 V and +0.76 V *vs.* Fc^+/Fc, irreversible).[33] For [Ag(dppb)$_2$][PF_6] (where dppb = 1,2-bis-(diphenylphosphino)benzene), $E^{ox}_{1/2}$ value of +0.48 V *vs.* Fc^+/Fc with a peak separation of 80 mV was reported (in MeCN)[34] and CV measurements of [Ag(dppb)$_2$][BF_4] in CH_2Cl_2 gave an oxidation potential of +0.99 V (SCE, quasi-reversible).[35] In contrast to the oxidation of the copper complexes, which are metal centred processes of the type Cu^+/Cu^{2+}, the oxidation processes of silver(I) compounds are usually ligand centred.

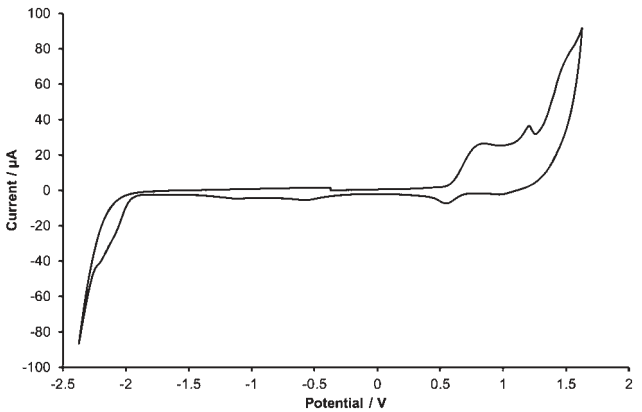

Fig. 3 Cyclic voltammogram of a CH_2Cl_2 solution of [Cu(*t*Bu-xantphos)(bpy)][PF_6] (*vs.* Fc^+/Fc, [^{n}Bu$_4$N][PF_6] supporting electrolyte, scan rate = 0.1 V s^{-1}).

Table 1 Cyclic voltammetric data for [Cu(*t*Bu-xantphos)(bpy)][PF_6] complexes and [Ag(*t*Bu-xantphos)(bpy)][PF_6] referenced to internal Fc/Fc^+ = 0.V; CH_2Cl_2 (freshly distilled) solutions with [^{n}Bu$_4$N][PF_6] as supporting electrolyte and scan rate of 0.1 V s^{-1}. Processes are quasi-reversible unless otherwise stated (ir = irreversible)

Complex cation	$E^{ox}_{1/2}$/V	($E_{pc} - E_{pa}$/mV)
[Cu(*t*Bu-xantphos)(bpy)]$^+$	+0.70	270
[Cu(xantphos)(bpy)]$^+$ [a]	+0.76	110
[Cu(*t*Bu-xantphos)(6-Mebpy)]$^+$	Only red. peak at +0.57 visible	ir
[Cu(*t*Bu-xantphos)(4,4′-*t*Bu$_2$bpy)]$^+$	+0.62	370
[Ag(*t*Bu-xantphos)(bpy)]$^+$	+0.87	90
*t*Bu-xantphos	Ox1: Only ox. peak at +0.46 visible; Ox2: +0.96	Ox2: 330

[a] Data from ref. 14.

Photophysical properties

Each of the solution absorption spectra of the heteroleptic copper(I) complexes and of [Ag(*t*Bu-xantphos)(bpy)][PF_6] exhibits the most intense band around 230 nm, followed by a second band at ~280 nm with shoulders (see Fig. 4). In contrast to analogous copper(I) complexes with xantphos or POP, the broad band typically around 360 to 440 nm, which is assigned to MLCT transitions,[11] is missing. Rather than the typical yellow colour of [Cu(POP)(N^N)(PF_6)] or [Cu(xantphos)(N^N)(PF_6)] complexes, solutions of [Cu(*t*Bu-xantphos)(N^N)(PF_6)] compounds (1.0×10^{-4} mol dm^{-3}) appear colourless by eye. For [Ag(P^P)(N^N)]$^+$ complexes the absence of an MLCT band in the visible area is the norm[18,30] rather than the exception.[19] In the solid state, however, the copper(I) complexes exhibit colours from bright yellow to orange and the signifi-

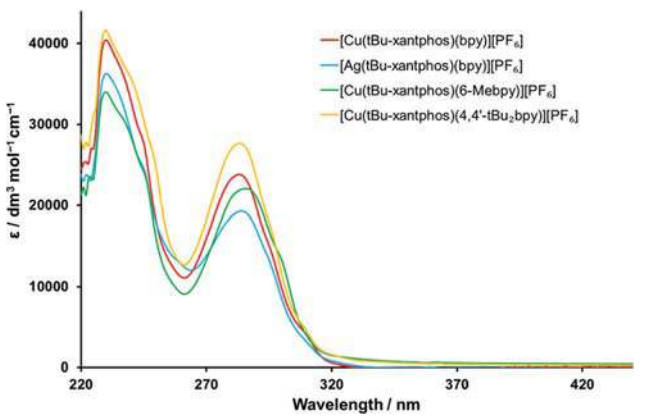

Fig. 4 Solution absorption spectra of the [Cu(*t*Bu-xantphos)(bpy)][PF_6] complexes and [Ag(*t*Bu-xantphos)(bpy)][PF_6] (CH_2Cl_2, 2.5×10^{-5} mol dm^{-3}).

Table 2 Emission maxima and photoluminescence quantum yields (PLQY) for the [Cu(*t*Bu-xantphos)(N^N)][PF_6] complexes and [Ag(*t*Bu-xantphos)(bpy)][PF_6] in the solid state

Complex cation	λ_{em}^{max}/nm (powder)	PLQY/% (powder)	τ/ns (powder)
[Cu(*t*Bu-xantphos)(bpy)]$^+$	647[b]	0.4[b], 1.1[c]	25
[Cu(xantphos)(bpy)]$^+$ [a]	587[b]	1.7[b]	1300
[Cu(*t*Bu-xantphos)(6-Mebpy)]$^+$	622[b]	0.4[b], 0.9[c]	22 (828), 140 (71)[d]
[Cu(*t*Bu-xantphos) (4,4′-*t*Bu$_2$bpy)]$^+$	567[b]	0.4[b], 0.7[c]	46 (392), 589 (164)[d]
[Ag(*t*Bu-xantphos)(bpy)]$^+$	447[b], 470[b]	2.5[b], 1.8[c]	2.9 (676), 13 (57)[d]

[a] Published data.[14] [b] λ_{exc} = 365 nm. [c] λ_{exc} = 280 nm. [d] Biexponential fit using the equation $\tau_{1/2}(av) = \sum A_i\tau_i/\sum A_i$ where A_i is the pre-exponential factor for the lifetime; numbers in parentheses are values of A_i.

cantly more concentrated solutions (0.02 mol dm^{-3}) used for NMR spectroscopic measurements are yellow.

None of the complexes shows a detectable emission in CH_2Cl_2 solution (both non-deaerated and deaerated). Even in the solid state, where the complexes are in a rigid environment and solution related quenching processes do not occur, the emissions are very weak for all complexes. The PLQY values are ≤1% for the copper(I) complexes with *t*Bu-xantphos and 2.5% for [Ag(*t*Bu-xantphos)(bpy)][PF_6] (Table 2). For the silver(I) complex, the excited state lifetimes are extremely short (bi-exponential, 2.9 and 13 ns, respectively), which implies that the emission is ligand based. The copper complexes with *t*Bu-xantphos are longer (22 to 589 ns), consistent with involvement of the metal centre, but are still shorter than the lifetime (1300 ns) of the reference compound [Cu(xantphos)(bpy)][PF_6][14] with the xantphos ligand bearing phenyl substituents. The emission spectra are illustrated in Fig. S13† and Fig. 5 (normalized), with the emission maxima listed in Table 2.

Comparison of the non-normalized spectra in Fig. S13† underlines how weakly emissive the copper(I) complexes are with respect to [Ag(*t*Bu-xantphos)(bpy)][PF_6], whereas in Fig. 6 the normalization of the spectra illustrates the shift of the emission maxima. The most blue-shifted emission is exhibited by [Ag(*t*Bu-xantphos)(bpy)][PF_6]; the emission spectrum shows two maxima at 447 and 470 nm. For the copper(I) complexes, the emission maxima move to shorter wavelengths on going from bpy to 6-Mebpy to 4,4′-*t*Bu$_2$bpy.

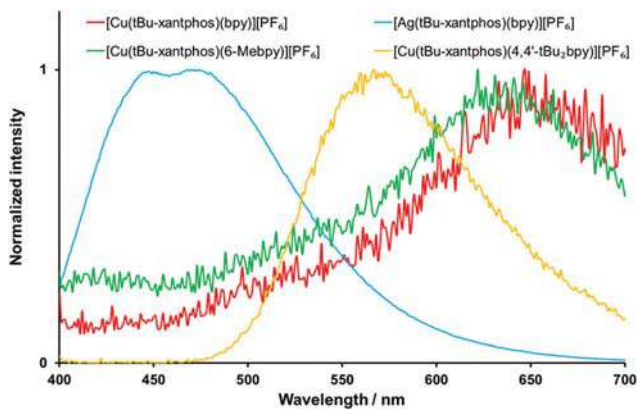

Fig. 5 Normalized emission spectra of the [Cu(*t*Bu-xantphos)(bpy)][PF_6] complexes in solid state.

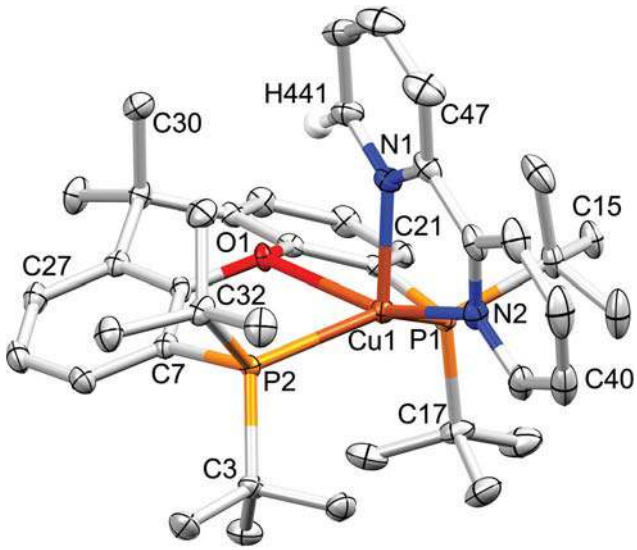

Fig. 6 Structure of the [Cu(*t*Bu-xantphos)(bpy)]$^+$ cation in [Cu(*t*Bu-xantphos)(bpy)][PF_6]. Ellipsoids plotted at 50% probability level, positions of H atoms refined, H atoms omitted except for H441 to show proximity to O1 (2.45(2) Å).

Discussion of vibrational quenching

In order to be a promising candidate as an emissive material in LECs or OLEDs, the iTMC needs to exhibit high PLQY values, which in turn means that non-radiative decay pathways should be minimized. A successful strategy to enhance the photophysical properties of copper(I) complexes is by stabilizing the tetrahedral geometry of the copper(I) centre, typically by introducing sterically demanding substituents which disfavours flattening of the coordination sphere in the excited state. Considering the steric crowding of four *tert*-butyl groups (see crystallography section), this was achieved in the case of [Cu(*t*Bu-xantphos)(bpy)][PF_6]. Thus, there has to be another origin for the almost complete quenching of the emission even in the solid state which is related to the *tert*-butyl groups. A possible recommendation for the design of emitting complexes to refrain from the incorporation of CH_2- and CH_3-groups in order to avoid vibrational quenching was found in the literature.[36] The C–H stretching modes are some of the highest frequency vibrations, with C_{sp^2}–H vibrations between 3100 and 3010 cm^{-1} and C_{sp^3}–H vibrations between 2950 and

2850 cm^{-1}.[37] The more vibrations that are present and the higher the energy of these vibrations, the easier it is to match an electronic gap with vibrational energy.[38] Although the C–H vibrations on the phenyl rings in xantphos are higher in energy than those of the *tert*-butyl groups in *t*Bu-xantphos, the number of C–H bonds in the former are fewer than in the latter (20 H in four phenyl substituents *versus* 36 H in four *t*Bu substituents). We have observed that *tert*-butyl groups introduced into the 4,4′-positions of the bpy ligand in [Cu(xantphos/POP)(4,4′-tBu$_2$bpy)]$^+$ do not lead to such a quenching effect,[39] and therefore we conclude that the closeness to the copper centre plays an important role in the quenching mechanism. One way to study the vibrational quenching is by making use of the isotopic effect. It has been shown that replacement of hydrogen atoms with deuterium in organic molecules leads to a reduction in vibrational quenching and enhancement of luminance;[33] a similar effect has been observed for some lanthanoid metal complexes.[40,41] The isotopic effect of the exchange of ^{12}C for ^{13}C has also been studied for the fullerenes C_{60} and C_{70}.[42] However, to the best of our knowledge, vibrational quenching effects in copper(I) complexes have not previously been described.

Steric and electronic properties of xantphos *vs.* *t*Bu-xantphos

Replacing substituents in phosphanes involves a change in both electronic and steric effects. A detailed study of steric effects of phosphorus ligands was published in 1977 by Tolman.[43] The Tolman cone angle Θ between the most outer atoms of a ligand and the metal centre is since then a ubiquitous parameter for assessing steric demand. A comparison of the cone angles of PPh_3 (145°) and $PPhtBu_2$ (170°)[44] indicates the significantly increased steric demand of the ligands *t*Bu-xantphos *vs.* xantphos. For complexes with chelating bisphosphanes the bite angle P–M–P is usually given as the main characteristic element. However, the two angles are correlated in that a chelating ligand with a wide bite angle also leads to a large cone angle, and *vice versa*. A useful parameter to compare chelating ligands independent from the coordinated metal is defined as the natural bite angle which describes the chelating angle as only determined by the backbone of the ligand.[45] Calculations using molecular mechanics show that the preferred bite angle of the phosphane ligand is also larger for *t*Bu-xantphos (140°) than for xantphos (108°).[46] In theory, an increase of these angles should lead to a decreased *s* character of the lone pair at the phosphorus. This is an example of how the electronic and steric effects are interlinked. While phenyl groups exhibit an inductive $-I$ effect together with a positive $+M$ effect, the $+I$ properties of the *tert*-butyl groups of *t*Bu-xantphos should also lead to an increased electron density at the phosphorus atom.

Structural characterization of the complexes

Single crystal X-ray diffraction quality crystals were obtained by layer crystallization, by slow diffusion of Et_2O into CH_2Cl_2 solutions of the complexes. The single crystal structures of the *t*Bu-xantphos[47] and xantphos ligands[48] have been reported.

Structures at ambient pressure

[Cu(*t*Bu-xantphos)(bpy)][PF_6] crystallized in the monoclinic space group $P2_1/c$, and the structure of the cation is illustrated in Fig. 6. Unexpectedly, the copper(I) atom is five-coordinate with the *t*Bu-xantphos ligands showing κ^3 binding from the phosphorus atoms and, in addition, from the oxygen donor of the xanthene unit with a short Cu–O distance of 2.6699(11) Å. Although these type of bisphosphanes with phenylether backbones are usually found in a bidentate chelating mode (κ^2), due to the ability of the oxygen to coordinate, similar geometries as in complexes with traditional PCP or PNP pincer ligands have been reported.[49] Both the Cu–P distances (Cu1–P2 = 2.3522(5) Å; Cu1–P1 = 2.3283(4) Å) as well as the Cu–N distances (Cu1–N2 = 2.1725(14) Å; Cu1–N1 = 2.1366(14) Å) are longer than in [Cu(xantphos)(bpy)][PF_6] (see Table 3). The central ring of the xanthene unit is in the boat conformation, as also found in the structure of [Cu(xantphos)(bpy)][PF_6].[14] Comparison of the fold angles, which are the angles between the mean planes that contain the outer aromatic rings of the xanthene backbone, gives values of 39.08° for [Cu(*t*Bu-xantphos)(bpy)][PF_6] and 32.40° for [Cu(xantphos)(bpy)][PF_6], thus revealing that the xanthene backbone is even less flattened in the former structure than in the latter (Table 3). The P–Cu–P chelating angle in [Cu(*t*Bu-xantphos)(bpy)][PF_6] (129.297(17)°) is significantly larger than in [Cu(xantphos)(bpy)][PF_6] (113.816(14)°), a trend which is in agreement with the aforementioned preferred bite angles (140° for *t*Bu-xantphos and 108° for xantphos).[41] With an ionic radius R_i of 0.60 Å (coordination number CN = 4), Cu^+ is relatively small in comparison to other metal cations (*e.g.* Ag^+, R_i = 1.00 Å for CN = 4),[50] which is reflected in short bond distances (Table 3). In order to stay within an efficient bonding distance, but also allow the bpy to coordinate to the copper centre, the folding of the xanthene backbone is required. Due to the steric crowding of the *tert*-butyl groups at the phosphorus atoms, the boat ring of the xanthene unit is folded towards the copper atom, thus allowing the oxygen to approach closely to the copper centre (Fig. 6). Another noteworthy feature is the position of the bpy ligand which is strongly tilted to the side and almost completely located above the xanthene backbone. The distance between the hydrogen H441 next to the nitrogen N1 of the bpy to atom O1 of the *t*Bu-xantphos ligand is 2.45(2) Å (Fig. 6) and this is consistent with a weak hydrogen-bonded interaction. However, while contributing to the tilting of the bpy, it is unlikely to be the driving force behind it.[51]

The structure of the cation in [Ag(*t*Bu-xantphos)(bpy)][PF_6], which crystallized in the triclinic space group $P\bar{1}$, is illustrated in Fig. 7 and an overlay with the structure of the copper analogue is shown in Fig. 8. The silver centre is coordinated in a distorted tetrahedral geometry with the angle between the *t*Bu-xantphos ligand and the bpy coming to 82.44°. As expected due to the larger atomic radius of silver, the Ag–P distances as well as the Ag–N distances are longer than in the respective copper cation (see Table 3). One of the most noticeable difference to the copper analogue is the almost flat geometry of the

Table 3 Comparison of structural parameters for the ligand *t*Bu-xantphos and its group 11 complexes

Compound	*t*Bu-xantphos	Xantphos	[Cu(*t*Bu-xantphos)][PF_6]·H_2O	[Cu(*t*Bu-xantphos)(bpy)][PF_6]	[Cu(xantphos)(bpy)][PF_6]	[Ag(*t*Bu-xantphos)(bpy)][PF_6]
CCDC number	255820	1303570	1583821	1583820	1581158	1583822
Colour	White	Colourless	Yellow	Yellow	Yellow	Colourless
Unit cell	Triclinic	Monoclinic	Orthorombic	Monoclinic	Monoclinic	Triclinic
	$P\bar{1}$	$P2_1/n$	*I2mm*	$P2_1/c$	$P2_1/n$	$P\bar{1}$
C–O–C angle/°	C4a–O1–C10a = 120.6(2)	C5–O1–C13 = 118.0(1)	C8–O1–C8 3_556 = 121.8(17)	C8–O1–C10 = 116.04(11)	C8–O9–C10 = 115.69(10)	C8–O1–C10 = 120.69(19)
Fused ring domain	Flat	Boat (feeble)	Flat but with disorder	Boat	Boat	Flat
Fold angle/°	0.63	20.13	0 (symmetry generated)	39.08	32.40	5.89
C_{ring}–P distance/Å	P1–C4 = 1.847(2);	P1–C6 = 1.838(2);	P1–C4 = 1.873(12)	P2–C7 = 1.8452(16);	P2–C3 = 1.8306(14);	P1–C11 = 1.845(3);
	P2–C5 = 1.850(2)	P2–C4 = 1.839(2)		C11–P1 = 1.8449(15)	C18–P19 = 1.8320(14)	P2–C3 = 1.839(3)
P–metal distance/Å	—	—	Cu1–P1 = 2.208(3);	Cu1–P2 = 2.3522(5);	Cu1–P2 = 2.2539(4);	Ag1–P1 = 2.5200(7);
			Cu1–P1 3_556 = 2.208(3)	Cu1–P1 = 2.3283(4)	Cu1–P19 = 2.2830(4)	Ag1–P2 = 2.5228(7)
O–metal distance/Å	—	—	Cu1–O1 = 2.253(14)	Cu1–O1 = 2.6699(11)	Cu1–O9 = 13.076(1)	Ag1–O1 = 3.035(2)
P–metal–P angle/°	—	—	P1 3_556–Cu1–P1 = 164.07(16)	P2–Cu1–P1 = 129.297(17)	P2–Cu1–P19 = 113.816(14)	P1–Ag1–P2 = 128.27(2)
N–metal distance/Å	—	—	—	Cu1–N2 = 2.1725(14);	Cu1–N44 = 2.1210(12);	Ag1–N1 = 2.606(2);
				Cu1–N1 = 2.1366(14)	Cu1–N55 = 2.0583(12)	Ag1–N2 = 2.514(2)
N–metal–N angle/°	—	—	—	N2–Cu1–N1 = 76.46(5)	N44–Cu1–N55 = 79.32(5)	N1–Ag1–N2 = 65.94(8)
Angle between ligands/°	—	—	—	89.56	79.63	82.44
O–metal–N angles/°	—	—	—	O1–Cu1–N2 = 162.55(5);	O9–Cu1–N44 = 96.47(4);	N1–Ag1–O1 = 148.14(7);
				O1–Cu1–N1 = 86.18(4)	O9–Cu1–N55 = 170.87(4)	N2–Ag1–O1 = 145.92(7)

Fig. 7 Structure of the [Ag(*t*Bu-xantphos)(bpy)]$^+$ cation in [Ag(*t*Bu-xantphos)(bpy)][PF_6]. Ellipsoids plotted at 50% probability level, H atoms omitted.

Fig. 8 Overlay of the crystal structures of the cations [Cu(*t*Bu-xantphos)(bpy)]$^+$ (dark orange) and [Ag(*t*Bu-xantphos)(bpy)]$^+$ (silver blue) with ellipsoids plotted at 50% probability level. Only the *ipso*-C atoms of the P*t*Bu_2 groups are shown and H atoms are omitted. The metallic centres of the cations were overlaid.

xanthene unit in [Ag(*t*Bu-xantphos)(bpy)][PF_6] (fold angle 5.89°). Furthermore, there is no bond from the oxygen of *t*Bu-xantphos to the silver centre, with the distance d(Ag–O) being 3.035(2) Å. While the P–Ag–P bite angle of 128.27(2)° is very close to the P–Cu–P bite angle, the longer Ag–P bonds allow for a flatter geometry of the xanthene backbone (Table 3).

The silver analogue also differs from the [Cu(*t*Bu-xantphos)(bpy)]$^+$ cation in terms of chelation by the bpy ligand. In contrast to the tilted coordination, the bpy in [Ag(*t*Bu-xantphos)(bpy)]$^+$ is almost perfectly opposite of the xanthene unit and by eye one might almost expect a mirror plane through the cation that cuts the bipyridine in half.

Crystallization setups of the mixture obtained from the reaction of [$Cu(MeCN)_4$][PF_6], *t*Bu-xantphos and 6-Brbpy yielded crystals of [Cu(*t*Bu-xantphos)][PF_6]·H_2O. The com-

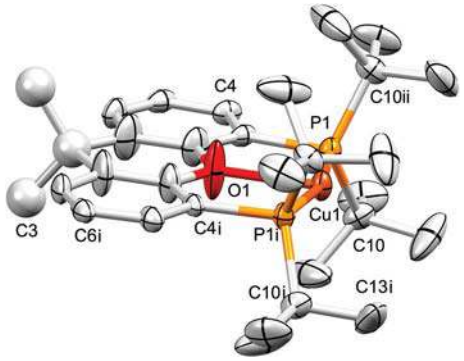

Fig. 9 Structure of the $[Cu(t\text{Bu-xantphos})(bpy)]^+$ cation in $[Cu(t\text{Bu-xantphos})(bpy)][PF_6]\cdot H_2O$. Ellipsoids plotted at 50% probability level, H atoms omitted. Symmetry generated atoms: i = *x*, *y*, 1 − *z*, ii = *x*, 1 − *y*, *z*. The CMe_2 group was refined isotropically (see text).

pound crystallizes in the orthorhombic space group *I*2*mm*, and the structure of the $[Cu(t\text{Bu-xantphos})(bpy)]^+$ cation is shown in Fig. 9. The copper atom is coordinated by one *t*Bu-xantphos ligand through two phosphorus atoms and the oxygen atom, no close contacts to the $[PF_6]^-$ anion or solvent molecules were observed. To our knowledge, this is one of the few structures where a copper(I) cation is only coordinated from one side by a chelating bisphosphane ligand. Other examples feature a P^N^P ligand with also either a *tert*-butyl or isobutyl group at the phosphorus atoms.[52,53]

Although the electron donating +*I* effect of the *tert*-butyl groups bonded to the phosphorus atoms might be expected to facilitate an oxidation to Cu(II), we observed that, even after weeks in non-deaerated solvents (CH_2Cl_2/Et_2O), no colour change was observed in the solid material of the crystallisation setup. This might be explainable by the packing in solid state: in the spacefill model of two $[Cu(t\text{Bu-xantphos})(bpy)]^+$ cations in Fig. 10 the packing shows that the methyl groups of the xanthene unit of the next cation almost fill the open "pocket" between the *tert*-butyl groups and therefore hinders the access to the copper centre, thus stabilizing the oxidation state +I.

The middle ring of the xanthene unit has a flat geometry, but the bridging CMe_2 carbon atom C9 and O1 possess a high thermal motion that might suggest some orientational disorder. C9 lies on the two mirror planes making it very difficult to investigate whether the disorder is real of just high libration. An attempt to model the possible disorder was made but did not lead to a reasonable solution. For this reason the CMe_2 group was refined isotropically. The $[Cu(t\text{Bu-xantphos})]^+$ cation is symmetry generated by a mirror plane through Cu1, O1 and the CMe_2 unit of the xanthene backbone. Another mirror plane goes through Cu1, the phosphorus atoms and the xanthene unit, which results in a *mer*-κ^3 coordination of the *t*Bu-xantphos ligand. The Cu–P bonds (2.208(3) Å) are shorter than in $[Cu(t\text{Bu-xantphos})(bpy)]^+$ and $[Cu(xantphos)(bpy)]^+$ and the same is true for the Cu–O bond (2.253(14) Å) (Table 3).

Structures at high pressure

The effect of increased pressure on the structures of $[Cu(t\text{Bu-xantphos})(bpy)][PF_6]$ and $[Ag(t\text{Bu-xantphos})(bpy)][PF_6]$ was studied by single crystal X-ray diffraction of crystals of the compounds in a diamond pressure cell. In order to assure that the pressure on the crystal is equivalent from all sides, hydrostatic conditions in the pressure cell were generated by flooding the cell with hexane. The change of the crystal parameters of $[Cu(t\text{Bu-xantphos})(bpy)][PF_6]$ was studied from 0.3 to 3.3 GPa. However the observed changes are only marginal (see Fig. 11 and Table S1†). The angle β increases with pressure from 98.56(2)° for 0.3 GPa to 99.44(3)° for 3.3 GPa. As expected, the lengths of the cell axes become shorter with increasing pressure, which is also reflected in the shrinking cell volume from 4064(3) $Å^3$ at 0.3 GPa to 3623(3) $Å^3$ at 2.3 GPa, which represents a reduced volume of 89%. In the last step, however, where the pressure is quite dramatically increased from 2.3 to 3.3 GPa, a phase change takes place. This results in a doubling of the cell axis *a* from 11.787(8) Å to 23.191(18) Å with a concomitant doubling of *Z* from 4 to 8.

In the case of $[Ag(t\text{Bu-xantphos})(bpy)][PF_6]$, the pressure study goes from 1.0 GPa to 4.5 GPa, but without the structure

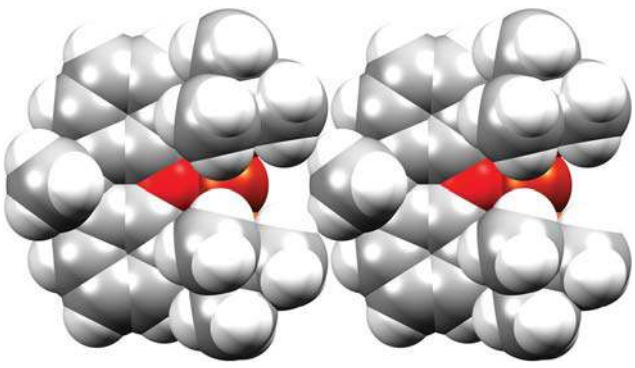

Fig. 10 Spacefill structure of the $[Cu(t\text{Bu-xantphos})(bpy)]^+$ cation in $[Cu(t\text{Bu-xantphos})(bpy)][PF_6]\cdot H_2O$.

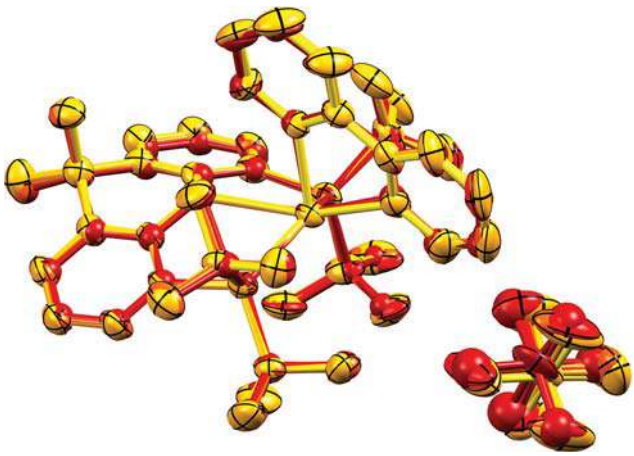

Fig. 11 Crystal structure of $[Cu(t\text{Bu-xantphos})(bpy)][PF_6]$ upon increasing the pressure from ambient (yellow) to 2.3 GPa (dark red). Ellipsoids plotted at 50% probability level, H atoms omitted.

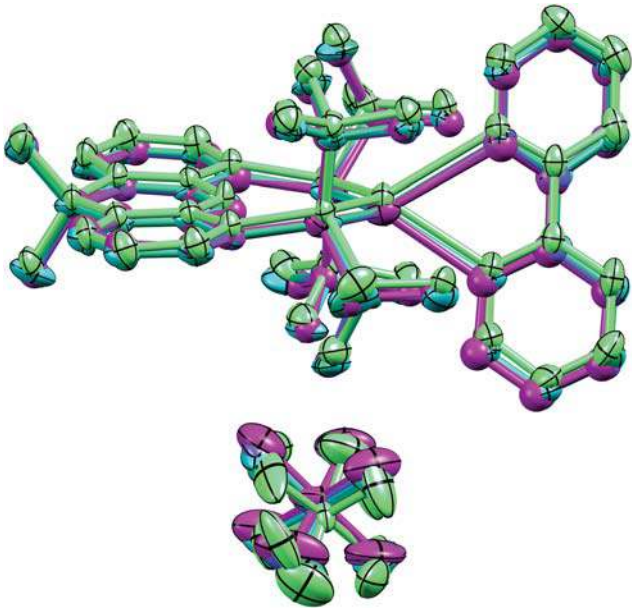

Fig. 12 Crystal structure of [Ag(*t*Bu-xantphos)(bpy)][PF_6] upon increasing the pressure from ambient (green) to 4.5 GPa (purple). Ellipsoids plotted at 50% probability level, H atoms omitted.

undergoing any phase change. As in the respective copper(I) complex, all cell axes decrease with augmented pressure, here resulting in a reduced cell volume of 91% (see Table S2†). As the overlay in Fig. 12 shows, only minor changes in the structure take place.

For both structures, the high pressure study confirmed the rigidity of the packing as well as the stability of the ligand coordination.

Conclusions

A series of [Cu(*t*Bu-xantphos)(N^N)][PF_6] complexes with N^N = bpy, 6-Mebpy and 4,4′-tBu$_2$bpy as well as [Ag(*t*Bu-xantphos)(bpy)][PF_6] was synthesized. The solid state structures of [Cu(*t*Bu-xantphos)(bpy)][PF_6] and [Ag(*t*Bu-xantphos)(bpy)][PF_6] were investigated at ambient and high pressure (up to 3.3 and 4.5 GPa, respectively) using single crystal X-ray diffraction experiments. The structures underwent little change upon increased pressure. Attempts to synthesize [Cu(*t*Bu-xantphos)-(6-Brbpy)][PF_6] yielded [Cu(*t*Bu-xantphos)][PF_6] which was structurally characterized. While in [Ag(*t*Bu-xantphos)(bpy)][PF_6], the *t*Bu-xantphos ligand is only coordinated *via* the phosphorus atoms, in the structures with copper(I) the ligand adopts a *P*,*O*,*P*′-pincer type coordination. The photophysical properties of the compounds with *t*Bu-xantphos contrast with those of the corresponding xantphos containing complexes. The poorer emissive properties of the former are mainly attributed to the *tert*-butyl groups inducing vibrational C–H quenching of the emission. This prompts a future study of the isotope effect upon exchange of hydrogen for deuterium in alkyl groups at various positions on the ligands and the resulting influence on the photochemistry of the complexes.

Conflicts of interest

There are no conflicts of interest to declare.

Acknowledgements

We acknowledge the Swiss National Science Foundation (Grant number 162631) and the University of Basel for financial support. Furthermore we would like to thank Diamond Light Source for access to beamline I19 (MT15176) and especially Dr Dave R. Allan. Y. Maximilian Klein and Dr Andrea Pannwitz are thanked for their efforts to share the shift work at the Diamond Light Source.

Notes and references

1 A. Kitai, *Materials for Solid State Lighting and Displays*, John Wiley & Sons, West Sussex, United Kingdom, 2017.
2 N. Thejokalyani and S. J. Dhoble, *Renewable Sustainable Energy Rev.*, 2014, **32**, 448.
3 A. De Almeida, B. Santos, B. Paolo and M. Quicheron, *Renewable Sustainable Energy Rev.*, 2014, **34**, 30.
4 S. Tang and L. Edman, *Top. Curr. Chem.*, 2016, **374**, 1.
5 E. Fresta and R. D. Costa, *J. Mater. Chem. C*, 2017, **5**, 5643.
6 See for example: C. E. Housecroft and E. C. Constable, *Chem. Soc. Rev.*, 2015, **44**, 8386.
7 R. Czerwieniec, M. J. Leitl, H. H. H. Homeier and H. Yersin, *Coord. Chem. Rev.*, 2016, **325**, 2.
8 M. Elie, S. Gaillard and J.-L. Renaud, in *Light-Emitting Electrochemical Cells*, ed. R. D. Costa, Springer International Publishing AG, Cham, Switzerland, 1st edn, 2017, pp. 287–327.
9 Q. Zhang, T. Komino, S. Huang, S. Matsunami, K. Goushi and C. Adachi, *Adv. Funct. Mater.*, 2012, **22**, 2327.
10 F. Brunner, L. Martínez-Sarti, S. Keller, A. Pertegás, A. Prescimone, E. C. Constable, H. J. Bolink and C. E. Housecroft, *Dalton Trans.*, 2016, **45**, 15180.
11 S. Keller, A. Pertegás, G. Longo, L. Martinez, J. Cerdá, J. M. Junquera-Hernández, A. Prescimone, E. C. Constable, C. E. Housecroft, E. Ortí and H. J. Bolink, *J. Mater. Chem. C*, 2016, **4**, 3857.
12 M. W. Mara, K. A. Fransted and L. X. Chen, *Coord. Chem. Rev.*, 2015, **2**, 282.
13 C. L. Linfoot, M. J. Leitl, P. Richardson, A. F. Rausch, O. Chepelin, F. J. White, H. Yersin and N. Robertson, *Inorg. Chem.*, 2014, **53**, 10854.
14 S. Keller, F. Brunner, J. M. Junquera-Hernández, A. Pertegás, M.-G. La-Placa, A. Prescimone, E. C. Constable, H. J. Bolink, E. Ortí and C. E. Housecroft, *ChemPlusChem*, 2018, DOI: 10.1002/cplu.201700501.

15 W. Su, T.-J. Gong, X. Lu, M.-Y. Xu, C.-G. Yu, Z.-Y. Xu, H.-Z. Yu, B. Xiao and Y. Fu, *Angew. Chem., Int. Ed.*, 2015, **54**, 12957.

16 M. C. Haibach, D. Y. Wang, T. J. Emge, K. Krogh-Jespersen and A. S. Goldman, *Chem. Sci.*, 2013, **4**, 3683.

17 J.-Y. Hu, J. Zhang, G.-X. Wang, H.-L. Sun and J.-L. Zhang, *Inorg. Chem.*, 2016, **55**, 2274.

18 O. Moudam, A. C. Tsipis, S. Kommanaboyina, P. N. Horton and S. J. Coles, *RSC Adv.*, 2015, **5**, 95047.

19 M. Z. Shafikov, A. F. Suleymanova, R. Czerwieniec and H. Yersin, *Chem. Mater.*, 2017, **29**, 1708.

20 G. J. Kubas, *Inorg. Synth.*, 1979, **19**, 90.

21 M. Shaul and Y. Cohen, *J. Org. Chem.*, 1999, **64**, 9358.

22 G. S. Hanan, U. S. Schubert, D. Volkmer, E. Rivière, J.-M. Lehn, N. Kyritsakas and J. Fischer, *Can. J. Chem.*, 1997, **75**, 169.

23 *APEX2, version 2 User Manual, M86-E01078*, Bruker Analytical X-ray Systems, Inc., Madison, WI, 2006.

24 P. W. Betteridge, J. R. Carruthers, R. I. Cooper, K. Prout and D. J. Watkin, *J. Appl. Crystallogr.*, 2003, **36**, 1487.

25 I. J. Bruno, J. C. Cole, P. R. Edgington, M. K. Kessler, C. F. Macrae, P. McCabe, J. Pearson and R. Taylor, *Acta Crystallogr., Sect. B: Struct. Sci.*, 2002, **58**, 389.

26 C. F. Macrae, I. J. Bruno, J. A. Chisholm, P. R. Edgington, P. McCabe, E. Pidcock, L. Rodriguez-Monge, R. Taylor, J. van de Streek and P. A. Wood, *J. Appl. Crystallogr.*, 2008, **41**, 466.

27 S. A. Moggach, D. R. Allan, S. Parsons and J. E. Warren, *J. Appl. Crystallogr.*, 2008, **41**, 249.

28 I. Kantor, V. Prakapenka, A. Kantor, P. Dera, A. Kurnosov, S. Sinogeikin, N. Dubrovinskaia and L. Dubrovinsky, *Rev. Sci. Instrum.*, 2012, **83**, 125102.

29 D. M. Adams, R. Appleby and S. K. Sharma, *J. Phys. E: Sci. Instrum.*, 1976, **9**, 1140.

30 CrysAlisPro 1.171.38.41k (Rigaku OD, 2015).

31 I. Andrés-Tomé, J. Fyson, F. B. Dias, A. P. Monkman, G. Iacobellis and P. Coppo, *Dalton Trans.*, 2012, **41**, 8669.

32 T. E. Barder and S. L. Buchwald, *J. Am. Chem. Soc.*, 2007, **129**, 5096.

33 C.-W. Hsu, C.-C. Lin, M.-W. Chung, Y. Chi, G.-H. Lee, P.-T. Chou, C.-H. Chang and P.-Y. Chen, *J. Am. Chem. Soc.*, 2011, **133**, 12085.

34 S. Igawa, M. Hashimoto, I. Kawata, M. Hoshino and M. Osawa, *Inorg. Chem.*, 2012, **51**, 5805.

35 A. Kaeser, O. Moudam, G. Accorsi, I. Séguy, J. Navarro, A. Belbakra, C. Duhayon, N. Armaroli, B. Delavaux-Nicot and J.-F. Nierengarten, *Eur. J. Inorg. Chem.*, 2014, **8**, 1345.

36 L. Bergmann, D. M. Zink, S. Bräse, T. Baumann and D. Volz, Top. Curr. Chem., in *Photoluminescent Materials and Electroluminescent Devices*, ed. N. Armaroli and H. J. Bolink, 2016, vol. 374, p. 201.

37 C. E. Housecroft and E. C. Constable, *Chemistry: An Introduction to Organic, Inorganic and Physical Chemistry*, Pearson Education, Essex, 4th edn, 2010.

38 N. J. Turro, *Modern Molecular Photochemistry*, University Science Books, Sausalito, California, 1991.

39 S. Keller, PhD Thesis, University of Basel, 2018, http://edoc.unibas.ch/diss/DissB_12466.

40 C. Doffek, N. Alzakhem, C. Bischof, J. Wahsner, T. Güden-Silber, J. Lügger, C. Platas-Iglesias and M. Seitz, *J. Am. Chem. Soc.*, 2012, **134**, 16413.

41 I. Hemmilä, V.-M. Mukkala and H. Takalo, *J. Fluoresc.*, 1995, **5**, 159.

42 C. Baleizão and M. N. Berberan-Santos, *ChemPhysChem*, 2011, **12**, 1247.

43 C. A. Tolman, *Chem. Rev.*, 1977, **77**, 313.

44 J. A. Bilbrey, A. H. Kazez, J. Locklin and W. D. Allen, *J. Comput. Chem.*, 2013, **34**, 1189.

45 C. P. Casey and G. T. Whiteker, *Isr. J. Chem.*, 1990, **30**, 299.

46 M.-N. Birkholz, Z. Freixa and P. W. N. M. van Leeuwen, *Chem. Soc. Rev.*, 2009, **38**, 1099.

47 C. Mispelaere-Canivet, J.-F. Spindler, S. Perrio and P. Beslin, *Tetrahedron*, 2005, **61**, 5253.

48 S. Hillebrand, J. Bruckmann, C. Krüger and M. W. Haenel, *Tetrahedron Lett.*, 1995, **36**, 75.

49 G. M. Adams and A. S. Weller, *Coord. Chem. Rev.*, 2018, **355**, 150.

50 Ionic radii in crystals, in *CRC Handbook of Chemistry and Physics*, Internet Version 2005, ed. D. R. Lide, CRC Press, Boca Raton, FL, 2005, http://www.hbcpnetbase.com.

51 T. Steiner, *Angew. Chem., Int. Ed.*, 2002, **41**, 48.

52 J. I. van der Vlugt, E. A. Pidko, D. Vogt, M. Lutz and A. L. Spek, *Inorg. Chem.*, 2009, **48**, 7513.

53 S. B. Harkins, N. P. Mankad, A. J. M. Miller, R. K. Szilagyi and J. C. Peters, *J. Am. Chem. Soc.*, 2008, **130**, 3478.